Physics – Uspekhi **48** (11) 1161 – 1175 (2005)

INSTRUMENTS AND METHODS OF INVESTIGATION PACS numbers: **68.43.–h**, **82.56.–b**, **91.60.–x**

NMR potentials for studying physical processes in fossil coals

A D Alexeev, E V Ulyanova, T A Vasilenko

DOI: 10.1070/PU2005v048n11ABEH002011

Contents

Abstract. High-resolution, pulsed, and wide-line NMR studies of fossil coals are reviewed. Coal substance conversion due to outbursts is discussed. Results on water and methane interactions with coal substance, which provide insight into the dynamic characteristics of boundary water, the location of methane in coal structure, and water and methane's hazard implications for coal beds (gas- or geodynamic phenomena) are presented; these are shown to have potential for predicting and preventing life threatening situations.

1. Introduction

By the late 1960s, the explosive development of solid-state nuclear magnetic resonance (NMR) spectroscopy had allowed its diverse applications in physics, chemistry, and technology [1].

Solid-state NMR spectroscopy's application to coal studies has made it possible to control geodynamic phenomena (GP) in coal beds.

In almost all coal basins worldwide, liberation of methane in coal mines has repetitively led to underground explosions of methane – air mixtures resulting in numerous casualties among miners [2]. The largest number of dead was documented in Japan in 1942. A methane explosion killed 1549 people there. In 1974, 439 people were killed in the USA. In 1980, 459 miners were killed in Germany. In 1997, 67 people were killed in Russia, and in 2000, 80 people were killed in Ukraine. Over the last decades, sudden coal and gas outbursts have become a factor comparable to regularly occurring natural calamities killing people and resulting in huge economic losses. One of the largest accidents took place in the 'Yurii Gagarin' mine of the Donetsk coal basin. Fourteen thousand five hundred tons of coal instantaneously broke down into the drift with 900,000 m^3 of methane being released [3]. According to the incomplete data, in the twentieth century, around 100,000 miners died from GPs in mines worldwide.

NMR methods have made studies of coal – water and coal – methane interrelationships possible. The models developed have allowed us to predict outburst initiation and to explain the formation of outburst-dangerous situations by tracing changes in coal molecular structure and have led to the development of safe coal and methane mining practices.

2. The structure of coal

Before analyzing NMR spectra of different coals, let us briefly consider what coal really comprises. Coal is a complex natural multicomponent product with a broad spectrum of chemical composition and physical properties. Its molecular structure has formed from plant residues by long actions of biological and chemical factors at high pressures and temperatures. Coals are graded (see Table 1) according to the degree of their metamorphization. In present-day coal science, coal metamorphism, or carbonification, means a process leading to substantial changes in molecular composition and properties of fossil coal in the earth's crust. During metamorphization, the carbon content of coal changes from 78% to 98%. The structure of coal is conventionally divided into the crystalline part composed of aromatic hydrocarbon groups and carbon groups (crystallites), and the aliphatic part

A D Alexeev, E V Ulyanova, T A Vasilenko Institute for Physics of Mining Processes, National Academy of Sciences of Ukraine
ul. R Luxemburg 72, 83114 Donetsk, Ukraine
Tel./Fax (380-62) 311 52 85
Tel. (380-622) 90 49 08; (380-622) 90 32 34
E-mail: alexeev@oftpg.fti.ac.donetsk.ua;
ekaterina-ulyanova@yandex.ru

Received 27 June 2004, revised 1 February 2005
Uspekhi Fizicheskikh Nauk **175** (11) 1217 – 1232 (2005)
Translated by D V Belyaev; edited by A Radzig

Table 1. Coal grades [2]*

Property	L	G	F	C	SB	B	A
Volatile matter V^g, %	37	35–37	28–35	18–28	14–22	8–18	>8
Carbon content, %	78	81–85	85–88	88–89	90	91–94	94–98
Hydrogen content, %	5.3	5.2	5.0	4.7	4.3	3.9	3.2

* L — long-flame coal, G — gas coal, F — fat coal, C — coking coal, SB — sintering baking coal, B — blind coal, A — anthracite.

(linked hydrocarbon groups). More than 50 models of coal structure exist [4].

Since the late 1980s, the prevailing view on coal is that of a complex polymer structure [5]. Coal's structure comprises a variety of the types of macromolecules. The simplest polymeric molecule (a chain of many covalently bonded atomic groups) has tens of thousands of links. Chains may consist of links of different types, being heteropolymers and copolymers. Besides, branched macromolecules are also encountered. They appear when many chain macromolecules are linked together in space [6]. The presence of heteroatoms and a huge diversity of ways of positioning them in a polymer chain considerably complicates the structure of the coal macromolecules.

Around defective cross-links of polymer chains, crystal structures (aromatic carbon) are formed. As the metamorphization progresses, the aromatic carbon part grows, with the aliphatic part diminishing.

Despite the large number of models, they do not describe the whole diversity of the properties of coals of different grades or even of the same grade of coals from different beds. More attention is therefore given to the data on carbon, hydrogen, and oxygen distributions among structural functional groups, the recurring unit positions, and unit bonds [7]. Coal organic matter is assumed to be a set of molecules of different chemical compositions, connected together by numerous couplings, with electron donor – acceptor (EDA) couplings being the main ones. In coal organic matter, EDA couplings are brought about by heterogeneity of the electron density distribution in macromolecules. This is caused by the presence in coals of various functional groups containing heteroatoms (O, N, S) and carbon atoms with different valence electron hybridizations. Separate base units possess different sets of sections exhibiting electron – donor and electron – acceptor properties. The nature of these sections depends on the chemical structure of functional groups, their environment, the macromolecule aromaticity, and the degree of condensation of aromatic structures. The same functional groups may be both electron donors and electron acceptors. This leads to the formation of greater number of EDA couplings in coal.

NMR studies allow more accurate classification of coals with close chemical compositions, for even coals of the same geological age and coals similar in their petrographic and element compositions may differ with respect to their structural groups contents.

2.1 Evaluation of the structural properties of coals from ^{1}H-NMR data

Fossil coals were first studied by applying the NMR technique by Van Krevelen, Richards and Yorke [4, 8]. In ^{1}H-NMR solid-state spectra, structural hydrogen of dry coal produces a wide component with the line width ΔH_2 and with the second moment M^2. The second moment M^2 depends on the separation between hydrogen atoms in the coal structure. Hydrogen atoms in an aromatic ring are spaced farther than those in aliphatic chains, which is why it was found possible to determine the relationship between aliphatic and aromatic hydrogen in coals from M^2 measurements. At normal temperatures ($T = 296$ K), the lines of H_{ar}, H_{al}, and H_{OH} nuclei are practically impossible to resolve, but Van Krevelen showed that at temperatures below 110 K, the second moments M^2 of the spectra depend on the coal metamorphism [4].

The second moments are conveniently calculated in practice from the expression [9]

$$M^2_{\text{exp}} = \frac{c^2 \sum_n f_n n^3}{3 \sum_n f_n n} , \tag{1}$$

where c is the scale of partition in the dimensions of a magnetic field, f_n is the ordinate of the nth point, and n is the horizontal partition number of the spectrum.

Richards and Yorke [8] gave an expression for calculating the ratio P_a of an amount a of hydrogen in aromatic chains to an amount b of hydrogen in aliphatic groups, depending on the second moments M^2:

$$P_a = \frac{a}{b} = \frac{M^2_{\text{al}} - M^2_{\text{exp}}}{M^2_{\text{exp}} - M^2_{\text{ar}}} , \tag{2}$$

where M^2_{exp} is the second moment of the coal hydrogen NMR spectra, and $M^2_{\text{al}} = 174.2 \times 10^3$ (A m^{-1})^2 and $M^2_{\text{ar}} = 61.4 \times 10^3$ (A m^{-1})^2 are the second moments of protons in aliphatic and aromatic groups, respectively, obtained with the model compounds.

Since M^2_{exp} of Donbass fossil coals varies from 147.8×10^3 (A m^{-1})^2 to 81.2×10^3 (A m^{-1})^2, when the yield V^g of volatile matter drops from 39% to 5% [10], then, according to Richards and Yorke, aromatic carbon content grows from 0.75 to 0.98. That is, when metamorphization progresses, the coal structure becomes more ordered and the content of the (aliphatic) side groups reduces.

Since the M^2_{exp} value changes practically linearly from 147.8×10^3 (A m^{-1})^2 to 81.2×10^3 (A m^{-1})^2 when the carbon content of coal varies from 75% to 95%, then a 1% increase in carbon content results, on the average, in a reduction of M^2_{exp} by 3.2×10^3 (A m^{-1})^2. The relationship obtained may be used for estimating the carbon content

$$\text{C} = 75 + \frac{147.8 \times 10^3 M^2_{\text{exp}}}{3.2 \times 10^3} \,\% .$$

In practical calculations, M^2_{exp} is evaluated with an accuracy of better than 5%, and C magnitude is calculated with an error none the worse than $\pm(1\,\%)^2$ [11].

As metamorphization progresses, the fraction H_{al} of methyl and methylene hydrogen atoms decreases, and the fraction H_{ar} of aromatic hydrogen increases. The total organic hydrogen content H_O is the sum of aromatic H_{ar}, aliphatic H_{al} and hydroxyl H_{OH} hydrogens. The hydrogen

distribution in H_{ar}, H_{al}, and H_{OH} is calculated by an equation resulting from the modification of that in Ref. [8]:

$$M^2_{exp} = \frac{a_1}{a_1 + a_2 + a_3} M^2_{ar} + \frac{a_2}{a_1 + a_2 + a_3} M^2_{al} + \frac{a_3}{a_1 + a_2 + a_3} M^2_{OH}, \quad (3)$$

where $a_1 + a_2 + a_3 = 1$, and a_1, a_2, and a_3 are the H_{ar}, H_{al}, and H_{OH} fractions, respectively.

Since $H_O = H_{ar} + H_{al} + H_{OH}$, then one finds

$$H_{ar} = a_1 H_O, \quad H_{al} = a_2 H_O, \quad H_{OH} = a_3 H_O;$$

M^2_{ar} and M^2_{al} are obtained from the model aromatic and aliphatic structures. M^2_{OH} magnitude is practically the same as that of M^2_{ar}[11].

2.2 The application of ^{13}C-NMR method to coal structure studies

Following the substantial development of solid-state ^{13}C-NMR technique, more complete and thorough structural studies of coal became possible. The first results of such studies were published in 1976 [12].

Since then, solid state NMR is being used to analyze coals and shales from different fields. The first studies had used moderate (1.4–2.3 T for 15–25 MHz) magnetic fields and had therefore produced data of low resolution. The spectra displayed two absorption maxima corresponding to aliphatic and aromatic bonds [11].

Improved high-resolution solid-state NMR-spectroscopy techniques realized in NMR spectrometers with strong magnetic fields (such as the 'Varian' and 'Bruker') have made better resolution of spectral lines possible [13].

Japanese authors [14] studied Australian brown coal containing 66.1% C, 5.3% H and 27.7% O in the combustible fraction. A Bruker CXP-300 spectrometer with a resonance frequency 75 MHz and rotor rotational frequency 4 kHz was used, and therefore the spectral resolution obtained was much higher than in earlier works. Absorption peaks corresponding to ten carbon-containing compounds were resolved in the ^{13}C-NMR spectrum (Fig. 1) [14].

The peaks produced by carboxyl (COOH) groups, oxygen-bound aromatic carbons (Ar–OH), aromatic carbons bound to alkyne ethers (Ar–OR) of hydroaromatic, ether, methylene (CH_2), and methyl (CH_3) groups are resolved well in the spectra. The spectrum changes dramatically after pyrolysis at 500 °C. In the aliphatic part, the resonances brought about by methyl and methylene groups completely disappear. In the aromatic part, the resonance line intensities increase sharply. These peculiarities are explained by an increase in aromatic carbon content during pyrolysis. The absorption maximum due to phenolic carbon remains the same. It is strong magnetic fields that allow us to get the so detailed picture of coal structures and detect changes in it during the process of coal treatment.

The authors of Ref. [15] used a Varian XL-200 NMR spectrometer to study several brands of New Zealand coals containing 62–92% C, 4.7–3.9% H, and 28.5–3.9% O. The ^{13}C-NMR spectra of all coals displayed several absorption peaks, thus confirming the conclusion of the authors of Ref. [14] that ^{13}C-NMR spectra give more detailed information about coal structure than its simple classification by aromatic and aliphatic parts.

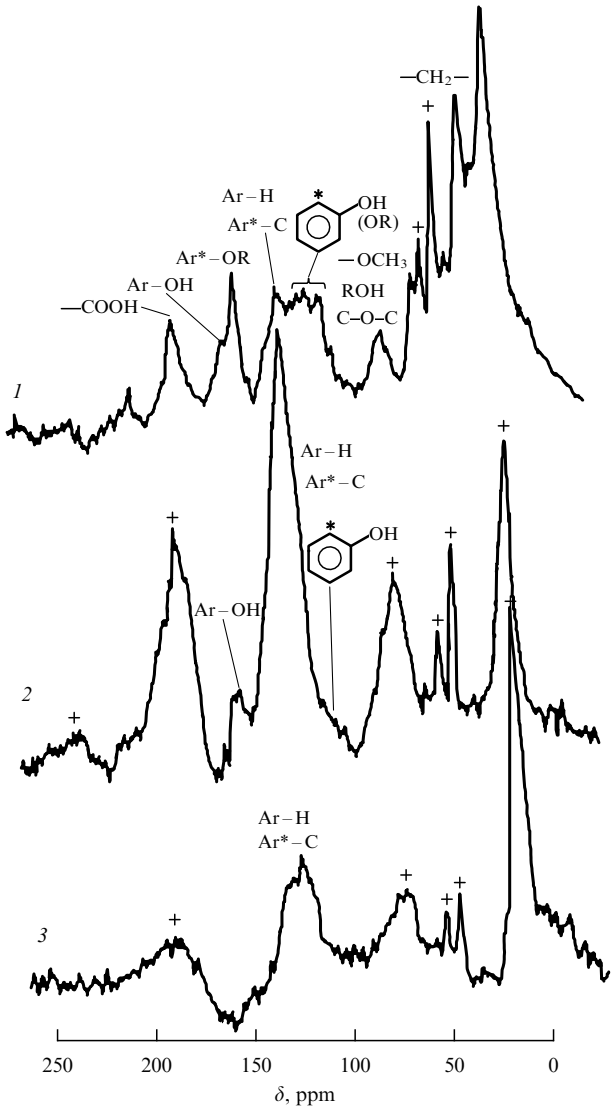

Figure 1. The spectra of Yallourn coal [14]: *1* — fossil coal; *2* — coal annealed at 773 K; *3* — coal annealed at 1073 K.

2.3 Studies of Donetsk coals

^{13}C-NMR spectra show not only the coal structure changes caused by various degrees of metamorphism but also the structural changes in coals of the same class, brought about by an outburst.

Using a Bruker CXP-200 spectrometer, the ^{13}C-NMR spectra of the Donetsk basin fossil coals of various degrees of metamorphization were recorded and the coal molecular structure differences before and after the outbursts were investigated [16]. The measurements were taken at room temperature. The operating frequency ran into 200 MHz. A standard technique of cross-polarization with a sample rotation at a magic angle was used. The mushroom-shaped rotor was made of deuterated plastic. The rotor rotational frequency ran into 3.5 kHz. The 90-degree polarizing pulse was 12×10^{-6} s long. The polarization transfer time reached 2×10^{-3} s. The phase of the first (polarizing) pulse changed 180° at each subsequent scanning, with the free induction decay polarity being inverted simultaneously. Thus, the overall signal was free from coherent errors. The repetition rate amounted to 512. The scanning time equalled 1 s.

The coal grades F (C = 84.8%), C (C = 88.5%), B (C = 89.7%), and A (C = 92.2%) were studied. The spectra

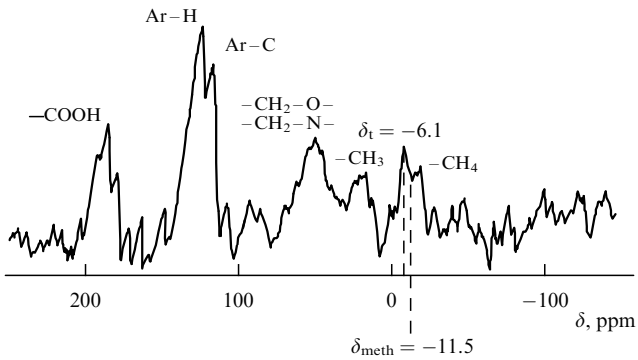

Figure 2. The ^{13}C-NMR spectrum of methane-saturated coal of grade L [17].

comprised four peaks. Some functional groups were identified by their chemical shifts (relative to the model compounds) [16]. The strongest absorption maximum attributed to heteroaromatic and aromatic hydrocarbons fell on 126 ppm. Carbon atoms are linked to oxygen, nitrogen, and sulfur heteroatoms through bridge bonds and exhibit absorption in a 72 ppm area. The absorption in the 18 and 20 ppm ranges is due to the presence of methyl-group carbon atoms in coal. In grade F coals, a peak at 30 ppm is caused by the presence of larger number of carbon atoms in methyl groups and methylene bridge groups, which are bound to nitrogen and halogen atoms. Absorption in the 176 – 200 ppm range is related to the presence of carbonyl groups of aldehydes and amide groups in coal.

Figure 2 [17] depicts the ^{13}C-NMR spectrum of a grade B coal saturated with methane. Besides four absorption peaks attributed to coal organic, an absorbed methane peak is also present. The chemical shift of absorbed methane varies from −4.2 ppm in the L grade to −9.3 ppm in the A grade. The chemical shift of gaseous methane is equal to −11.5 ppm. The chemical shift of the first molecular layer varies from −7 ppm to +5 ppm [18].

NMR spectra of coal samples taken from stable regions (pillars) of a bed and from outbursts of the same bed proved to be considerably different. In outburst coals, the spectral line intensities in the 127 ppm range are reduced, pointing to detachment of light hydrocarbons attached to the aromatic part of coal [16]. Significant reductions of 20 ppm and 73 ppm absorption maxima indicate a decline in the number of aliphatic chains due to many bond disruptions during outbursts. Natural coal exhibits the main properties of polymers [19]. Polymer deformations, for instance, result in molecular restructuring and are accompanied by gas releases. By drawing an analogy between breakages of polymers and coals, the authors of Ref. [17] conclude that coal structure disruption during an outburst is accompanied by methane production. This explains the huge release of methane during outbursts, exceeding the effective methane capacity of the bed. This was somewhat later confirmed in Refs [20, 21].

3. Humidification of coal beds as a means of outbursts prevention

3.1 The coal porosity

In coal research, one needs to account for the water and gases (CH_4, CO_2, heavy hydrocarbons) that coal is saturated with. Gases and water are by-products of the process of coal substance formation (coalification). During coalification, starting plant cells lose some hydrogen and oxygen in the form of water, methane, and other gases. Characteristically, methane dominates the Donetsk coals. The pressure of the upper rocks and the released gaseous products produced a peculiar disperse structure of fossil coals with pores and cracks spanning the size range of seven orders of magnitude: from methane (0.414 nm) and water molecular sizes to cracks that are several millimeters wide. Pores differ from cracks in that their sizes in all three dimensions are comparable. A crack size measured in one direction may differ from its size in the other two directions by several orders of magnitude. Pores play an important role in the coal structure and are classified into three groups with quite different properties: micropores (less than 1nm in diameter), intermediate pores (from 1nm to 10 nm), and macropores (over 10 nm across). Pores are divided into open pores (connected to each other and to the exterior surface of mineral) and closed pores (not connected to the exterior surface).

Research into coal porosity and the related sorptive properties is of practical importance, because the main problems of coal mining are how to prevent sudden outbursts and to fight with explosions of the air – methane mixtures of gas and coal. These problems are related to the amounts of water that is already present in the coal and artificially pumped to the coal masses, to various surfactants, and to the amount and the phase state of the methane.

Consider the effects of water and surfactants on coals of different degrees of metamorphization. Academician S A Khristianovich et al. [22] mathematically described the development of the outburst-dangerous situation in a coal bed by intergrowth of gas-filled pores and cracks. It was proven that even with due account of the mean gas pressure, the cracks intergrowing in a bed at the instant of the pressure relief of strained coal in the vicinity of the working face may lead to the development of rupture planes behind the squeezing zone, parallel to the face and filled with gas — that is, to an outburst-dangerous situation. The required surfactants must, upon their introduction in the coal masses, ensure the development of cracks through the involvement of the rock pressure due to the Rebinder effect. Since cracks in an intact coal bed are randomly distributed and there is no dominant bearing pressure, they will equiprobably develop in all directions.

When the second working face approaches a surfactant-treated zone, gas drains in the channel network and is locked in dead-end pores due to the higher sorptive ability of coal to water than to methane. Besides, the introduction of surfactant solutions plastifies the coal bed and increases the squeezing zone. In other words, the probability of the occurrence of an outburst event is lower [23, 24].

The effectiveness of the humidification as a way to fight with gas and coal outbursts depends on adsorbed (physically bound to the coal surface) water, not on the total amount of water pumped into the bed. Only physically bound water affects the strength of coal, its gasodynamic properties, and its potential for outburst [25, 26].

3.2 Water physically adsorbed by coal

Physical adsorption shows itself in the increase of a substance (water, in our case) concentration on a surface of solid body (on the surface of a coal pore), resulting from the substance attraction and retention at a phase boundary by Van der Waals forces. Physically adsorbed molecules keep their chemical

identities and adsorption is reversible. The nature of the surface greatly influences the character of intermolecular interactions and the boundary phase properties.

Since the fundamental thermodynamics work of Gibbs [27] much attention has been paid to the problem of fluid structure at interfaces. Due to its unique properties, water occupies a special place in fluids and the problem of water structure at interfaces has always interested scientists [28]. Numerous studies in this field have shown that water structural and dynamic properties at an interface are significantly different from those of the bulk fluid [29, 30]. It is worth noting that boundary layers are formed not only by adsorbed water but by all fluids [31]. However, the polymer-like structure of water and the presence of cooperative network of hydrogen bonds affect the boundary phase properties. Research on how the nature of intermolecular interactions and the type of surface influence interface properties has also begun to play an important role.

In earlier studies of bound water, the boundary layers were assumed to be fairly thick, namely, 10^2-10^3 nm [32]. These values were later found to be significantly overestimated. Some researchers supposed that the boundary layer thickness d_b does not exceed $\sim 10-100$ nm [33], but in subsequent studies d_b was shown unlikely to exceed $1-2$ nm [34]. One of the characteristic features of the water boundary layer is the orientation ordering of water molecules near the interface that gives rise, particularly, to the surface potential jump [28].

The work by Rideal [35], De Boer [36], and his disciples [37] played a major role in the development of views on adsorbed molecule motion. Out of various models for the monomolecular adsorption layer, De Boer [36] has chosen two extreme cases of the localized adsorption and the delocalized adsorption. The localized adsorption model implies that adsorbed molecules are strongly bound to the adsorption centers; they do not possess translational degrees of freedom and vibrate neither in a transverse nor in a longitudinal direction to the surface. It was repeatedly stressed [36] that the localized character of adsorption does not mean that the adsorbed molecules always remain at rest. The mere fact of gas–adsorption layer equilibrium points to the transverse molecular motion, not to mention the longitudinal molecular motion.

Adsorbed molecules migrate across the surface by jumping from one adsorption center to another. The Frenkel equation [38] links the molecule residence time τ_c in one section with the molecular activation energy V_0 for a molecule executing a jump-like motion across the surface:

$$\tau_c = \tau_0 \exp\left(\frac{V_0}{RT}\right), \tag{4}$$

where τ_0 is a constant related to the vibration period of the adsorbed molecule. The quantity V_0 is the difference between the heat of molecular adsorption on a surface active center and that onto the surface section between two active centers. Therefore, V_0 is significantly lower than the heat of adsorption Q. For physical adsorption by hydrophilic (polar) surfaces, the V_0 value is usually $1/3-1/2$ of $Q \geqslant 40$ kJ mol^{-1} [39]. This is considerably greater than the thermal motion energy $RT \sim 2.4$ kJ mol^{-1} at $T = 290-295$ K. The molecule residence time τ_c therefore exceeds the vibration period τ_0 being of the order of 10^{-13} s but is known to be shorter than the adsorption time t. Examples given in Refs [36, 39] show that for the physical adsorption by polar adsorbents the t/τ_c ratio is ~ 5000. If V_0 is lower than the energy of thermal motion, then the adsorbed molecules freely move across the surface in two directions. The adsorption layers composed of such molecules behave like a two-dimensional gas. In this case, adsorption is described by the delocalized model. According to De Boer [36], the adsorbed molecules maintain the rotational and two translational degrees of freedom at the ideal delocalized adsorption.

The surface of polar adsorbents is usually heterogeneous with respect to its energy [40]. As heterogeneity increases, the distribution of molecules among different adsorption centers is no longer equiprobable, and the impact of the combinatory term in the total entropy of adsorption is reduced. In other words, no model may account for all the diversity of peculiarities for real adsorption systems [41].

When analyzing the adsorption entropy of real systems, the reduction in the number of rotational degrees of freedom is also taken into consideration along with the partial or full translational immobility of adsorbed molecules, because the surface produces a potential barrier that restricts molecular rotations. In the context of the results discussed above one should note that at any hydrophilic surface water molecules are adsorbed in localized manner — that is, they interact with the surface polar groups.

Over time, scientists have paid more attention to the research on water adsorption onto the surfaces of hydrophobic materials [42, 43]. Almost all hydrophobic adsorbents have hydrophilic adsorption centers on their surfaces. Their active centers are various π-bonds, lone electron pairs, small-radius cations, oxygen-containing groups, and CH, CH_2, and CH_3 radicals. It is the hydrophilic centers that primarily adsorb water molecules. This results in localized water adsorption on coals with a small degree of surface filling.

However, no data on the molecular state of water adsorbed by hydrophobic adsorbents with different concentrations and polarities of their hydrophilic centers exist in the literature. This is to some extent related to the experimental difficulties of measuring the number of hydrophilic groups on the hydrophobic adsorbent surfaces by techniques that are independent of the water adsorption measurements, not to mention the difficulties in the intentional production of specific adsorption centers of different polarities on the surfaces of such adsorbents.

Among the instrumental methods for researching the structure and dynamics of boundary water, the broad-band NMR and the pulse NMR stand out. These methods are widely used for studies of the water state in various heterogeneous systems [44, 45].

3.3 ^{1}H-NMR wide-line spectroscopy of fossil coals

In wide-line NMR spectrometers, the modulation (autodyne) method is often used for raising the sensitivity and accuracy of measurements. The polarizing magnetic field H_0 is superimposed by the oscillating field $H_m \cos \omega t$. To avoid NMR spectral aberrations [46], the oscillating field amplitude M must be within the following range

$$\frac{\Delta H}{10} \leqslant M \leqslant \frac{\Delta H}{2}, \tag{5}$$

where ΔH is the spectral line width.

The resulting NMR spectra of coal-water, coal-methane, and coal-water-methane systems are the first derivatives

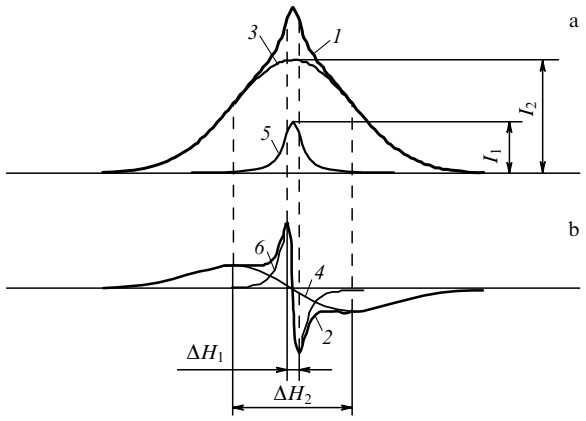

Figure 3. An NMR absorption line of a fluid-containing solid (a), and the first derivative of the absorption line (b) [47]: *1* — absorption spectrum; *2* — the first derivative of the absorption spectrum; *3* — the wide component of the absorption spectrum; *4* — the wide component of the first derivative of the absorption spectrum; *5* — the narrow component of the absorption spectrum; *6* — the narrow component of the first derivative of the absorption spectrum. I_1 and I_2 — intensities, ΔH_1 and ΔH_2 are the widths of the narrow and wide lines in an NMR spectrum, respectively.

(Fig. 3b) of the absorption lines (Fig. 3a) and consist of two superimposed lines, a narrow line and a wide line. Hydrogen atoms inherent in coal structure give rise to the wide line, and the hydrogen of water and methane gives rise to the narrow line. The quantity ΔH depends on the ^{1}H nuclei mobilities in the system in question. The line widths ΔH_1 and ΔH_2 of the narrow and wide components of an NMR spectrum, respectively, are different by an order of magnitude, for in real materials atomic nuclei interact with each other and with other carriers of magnetic moments (other atomic nuclei, atomic electron shells, paramagnetic ions, etc.) in the material and, therefore, the external constant magnetic field H_0 is supplemented by local magnetic fields H_i. Thus, the magnetic field $H = H_0 \pm H_i$ acts on any atomic nucleus. H_i depends on the surrounding atom mobilities [48]. In fluids and gases, the internal magnetic fields always fluctuate, therefore, H_i is small and the resonance lines are sharp in fluids and, especially, in gases. The resonance line widths ΔH_1 of the adsorbed water and methane vary from 0.079 to 119.4 A m^{-1}, depending on nucleus mobilities, and the spectral line width (ΔH_2) relevant to coal organics varies from 437.7 A m^{-1} to 517.3 A m^{-1}, depending on the degree of metamorphization.

The modulating field amplitudes M are therefore different for a wide and narrow components of NMR spectra. The value of $M = 35.0$ A m^{-1} is used for obtaining a general spectrum of a coal – fluid system. In this case, the narrow line width ΔH_1 is deliberately distorted, but an opportunity appears for tracking the relative changes of both components of an NMR spectrum (see Fig. 3). The modulating field amplitude amounts to 8.0 A m^{-1}, when determining the true line width of the narrow spectral component.

The intensities I_1 and I_2 of the NMR spectral lines depend on the number of nuclei in resonance and on their mobilities. At the same number of resonating nuclei, I will differ at various mobilities [49].

The studies of water physically adsorbed on fossil coals began half a century ago [47, 50 – 52]. The dependence of the water adsorption on the degree of coal metamorphization was analyzed for all grades of Donbass coals. The work was done on naturally and artificially moistened coals [53, 54].

Table 2. The dependence of the narrow line width ΔH_1 of NMR spectra on the coal grade [47]*

Coal grade	L	F	C	B	A
ΔH_1, A m^{-1}	43.0	39.8	35.8	32.6	18.3

* L — long-flame, F — fat, C — coking, B — blind, A — anthracite.

Adsorption centers appearing in different grades of coal (the degree of carbonification is changed) are shown to possess different energetics [47]. ΔH_1 values relevant to adsorbed water in the first monolayer decrease as the metamorphization progresses (Table 2), with L grade coal (the first in a row of fossil coals) having the maximum ΔH_1 value, and anthracites having the minimal value.

The value of ΔH_1 decreases as the number of adsorbed layers grows. During artificial humidification of previously dried and degassed coals, the initial value of the natural moisture content is achieved. Since coal is hydrophobic, it is almost impossible to increase the coal moisture content above the natural value. For instance, the natural moisture content of the outburst-dangerous grade C (coking) and F (fat) coals is not high: $W = 0.9 - 1.3\%$. When artificial humidification of a bed is used as a means of fighting with outbursts, the effectiveness of humidification indeed depends on the quantity of physically adsorbed water. For instance, the value of W in a grade F coal must be equal to 2.0% [55].

The action of physically adsorbed water manifests itself in both wedging and weakening intermolecular bonds among coal particles at microcrack mouths. At the maximum moisture content, the sorptive forces of water interaction with a solid surface are able to convert coal mass into a plastic state and thus exclude the hazard of sudden outbursts. Therefore, the amount of coal-adsorbed water is one of the main indicators of the outburst-dangerous condition of a bed [56].

To determine the amount of adsorbed water needed for conversion from brittle to ductile fracture, the fracture of coals of different grades with different adsorbed-water content was studied and the outburst conditions were emulated using an experimental facility of uneven three-component compression. The water-containing specimens were 50 mm cubes [25]. The outburst conditions were emulated by varying the stresses σ_1, σ_2, and σ_3. It was found [26] that, depending on the coal grade, outbursts do not take place at a moisture content of 2 – 3%. Further moisture content increase is not rational. Extensive underground research [24] in different geological conditions confirmed that the given content of physically bound water is enough for the reduction of outburst-hazardous situations in coal beds.

3.4 Effects of surfactants on the adsorptive properties of coals

To prevent coal and gas outbursts, the regional method consisting in the preliminary humidification of beds through the deep shaft wells is employed. Here, a bed prone to outburst is in advance converted to the outburst-safe state in the treated zone. But the preliminary humidification by pumping water is limited only to beds with extensive fissuring and, therefore, good permeability. Generally, coal beds are hardly soaked with water. This is due to coal hydrophobicity and high water surface tension $K = 7.3 \times 10^{-3}$ J m^{-2}, thus making deep water penetration into the porous coal space impossible.

Adding surfactants to water is one way to facilitate the humidification of coals. Presence of surfactants in water reduces its surface tension to $K = 1.5\times10^{-3}$ J m^{-2}, thus significantly increasing the penetration of water into a coal bed. Since the early 1960s, surfactants have been used for improving water penetration into coal masses. But at the present moment, this problem is not completely solved. The reason for this lies in the impossibility of selecting one kind of surfactant for all coal grades [57]. Sometimes, the same surfactant works differently on the same coal grade in different mines. Besides, the cost of surfactants is quite high and this results in higher expenses for antioutburst measures. Therefore, surfactants are chosen out of new and existing ones for their good effectiveness at low concentrations.

To solve this problem there were chosen surfactants among those preliminary analyzed at the Kiev Institute of Colloid Chemistry and Water Chemistry of the Ukrainian Academy of Sciences; these surfactants considerably reduce water surface tension at concentrations 0.01% – 0.1%.

The most effective and cheapest surfactant is sulfanol. As soon as 24 hours after the coal treatment with 0.5% sulfanol solution, the adsorbed water content increases from the natural 0.95% – 1.3% to 2.5% [58]. This happens because the surfactant radicals group around the pore adsorption centers and themselves become adsorption centers for water molecules. In these conditions, the new centers possess higher activation energies than the initial centers. It is clearly seen from the NMR spectra. The NMR spectral line widths $\Delta H_{1\,\mathrm{sur}}$ of the surfactant solution are greater than $\Delta H_{1\,\mathrm{w}}$ of water at the same water content (see Table 3) [58]. This points to stronger binding of water to adsorption centers under the usage of surfactants.

Table 3. The dependence of ΔH_1 of grade C coals on water content [58].

W, %	1.0	1.5	2.0	2.7
ΔH_1, A m^{-1} (water)	33.4	27.8	—	—
ΔH_1, A м$^{-1}$ (surfactant)	58.1	47.7	42.9	39.8

The two-to-three-fold improvement in the plastic properties of coals with the elevated adsorbed moisture content to 2.0% – 2.5% allowed us to develop a procedure of preventive humidification of coal beds by aqueous surfactant solution for coal and gas outburst prevention [54, 58]. By using preventive humidification of coal beds with the surfactant solutions and by synchronous NMR-based control of the coal moisture content it was possible to make the most outburst-hazardous Donbass beds safeer and thus to mine them [18].

4. Mechanisms of moistened coal adsorption at low temperatures

The wide-line NMR method allows one to estimate the effects of the porous structure and active surface adsorption centers on the activation energy V_0 and correlation times τ_c. The method is easier than, for example, measurements of the entropy in a wide range of temperatures [59], dielectric losses at various frequencies, and the nuclear quadruple resonance (NQR) frequency [60].

Using the approximate theory of Bloembergen, Purcell, and Pound [61], information about the changes in correlation time τ_c characterizing the water molecule mobility were obtained from experimental data on low-temperature broadening of NMR lines in the spectra of adsorbed water. According to Waugh and Fedin [62], the molecular correlation time τ_c and the line widths ΔH and ΔH_0 at the given temperature and at the temperature of the rigid lattice, respectively, are related by

$$(\Delta H)^2 = \frac{2(\Delta H_0)^2}{\pi} \arctan \frac{\alpha\gamma\,\Delta H}{\omega_c}\,, \tag{6}$$

where ΔH_0 is the 'frozen' lattice line width; $\alpha = 8\ln 2$; $\gamma = 4258$ s^{-1} Oe^{-1}, and $\omega_c = 2\pi/\tau_c$ is the molecular reorientation frequency.

From here, the expression for the correlation time may be given as

$$\tau_c = \frac{2\pi}{\alpha\gamma\,\Delta H} \tan\left[\frac{\pi}{2}\left(\frac{\Delta H}{\Delta H_0}\right)^2\right]. \tag{7}$$

The low-temperature dependences of the line widths and the second moments were obtained for several coal grades in Refs [18, 63] (see Figs 4, 5). Low-temperature NMR spectra of coals are characterized by different temperatures of the phase transitions of the adsorbed water from the liquid to the crystal-like state for different coal grades (Fig. 6) [18]. The

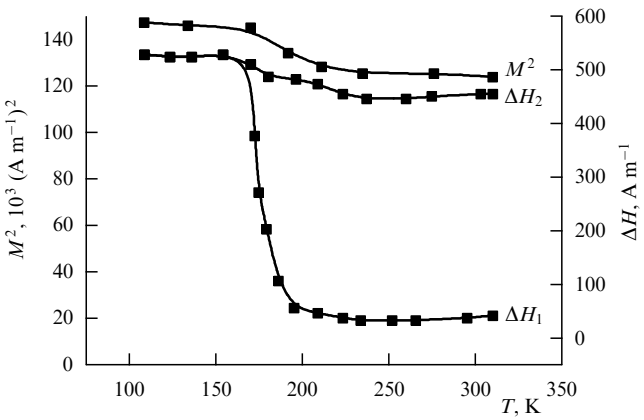

Figure 4. The dependences of line widths ΔH_1 and ΔH_2 and the second moments M^2 of NMR spectra of grade A coal on temperature ($V^g = 5\%$) [63].

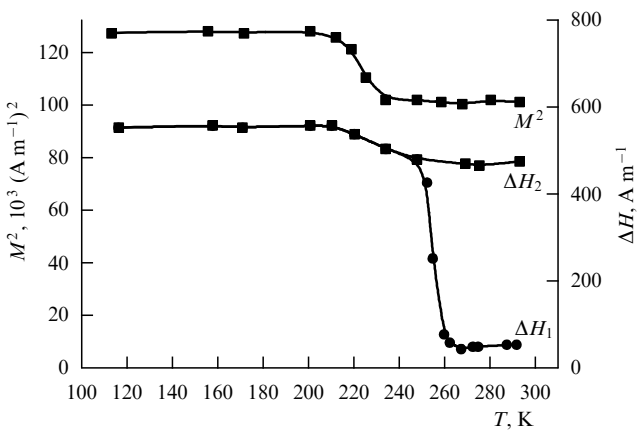

Figure 5. The dependences of line widths ΔH_1 and ΔH_2 and the second moments M^2 of NMR spectra of grade C coal on temperature ($V^g = 26\%$) [63].

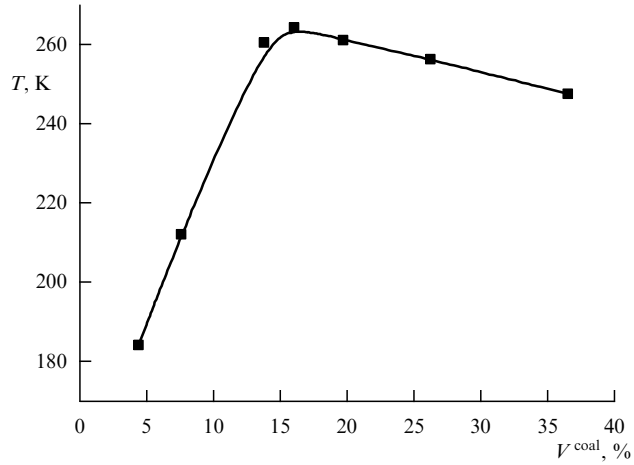

Figure 6. The dependence of the liquid – crystal-like phase transition temperature T of adsorbed water on the coal volatile matter V^{g} [18].

phase transition happens not sharply but continuously due to the firstly freezing of molecules less tightly bound to the surface. As shown by Blokh [64], two or three monolayers closest to the surface maintain their mobility down to rather low temperatures, when the rotational motion freezes. For anthracites, the transition begins at 183 K, for coals with $V^{\text{g}} = 26\%$ it begins at a temperature of 158 K, and for coals with $V^{\text{g}} = 39\%$ it begins at 233 K.

According to the Waugh – Fedin equation [62], the potential barrier V_0 of the retarded motion is simply given by

$$V_0 = 155.4\, T \text{ kJ mol}^{-1}\,, \tag{8}$$

where T is the phase transition temperature.

The maximal V_0 value of 40.74 kJ mol^{-1} is reached in coals with a volatile $V^{\text{g}} = 39\%$, and the minimal value of 28.43 kJ mol^{-1} in anthracites ($V^{\text{g}} = 5\%$). Thus, water molecules are most tightly bound to the surface adsorption centers of coals at the medium stage of metamorphization. As follows from Eqn (7), the molecular correlation time τ_{c} in coals with $V^{\text{g}} = 39\%$ equals 2.8×10^{-5} s at 233 K, in coals with $V^{\text{g}} = 26\%$ the same time is achieved already at 253 K, and in anthracites with $V^{\text{g}} = 5\%$, the correlation time is equal to 3.1×10^{-5} s at 173 K.

According to the De Boer classification, adsorption in coals of low and medium stage metamorphization belongs to localized adsorption. In anthracites, the water adsorption is closer to the delocalized adsorption.

5. Studies of porous coal structures by the pulse NMR method

The successful application of pulsed NMR method to studies of physically adsorbed water in coals is first of all explained by the fact that the correlation time of molecular processes in boundary water is generally longer than that in bulk water ($\tau_{\text{c}} \cong 3 \times 10^{-12}$ s) and falls into the maximum-sensitivity time interval of pulsed NMR, which ranges from 10^{-11} s to 10^{-6} s. Experimental data on spin – lattice (T_1) and spin – spin (T_2) relaxation times furnish an opportunity to obtain useful information about the dynamic characteristics of boundary water and, in particular, to calculate the molecular correlation times.

In addition, the NMR relaxation method proves to have a good potential for studying the porosity of coals, since the T_1 and T_2 quantities depend on the size, volume, and surface area of the pores and the extent of their filling [65].

Studying pore structure in coals is rather complicated due to the heterogeneity of the pores: micro- and macropores are present at the same time [66]. Although the largest amount of data has come so far from ^{1}H-NMR experiments, considerable difficulties still exist in interpreting T_1 and T_2 values for protons [65, 67, 68]. Therefore, silica gels have been used as the model adsorbent.

In the papers [69 – 71], the spin – spin relaxation time T_2 of water molecules adsorbed on silica gels with 0.9 nm, 0.25 nm, 1.4 nm, and 6.5 nm pores and also in coals of different grades (L, B, and A) was measured.

The T_2 value for water protons was measured at $T = 298$ K and on a frequency of 20 MHz. A two-pulse method was applied ($90° < \tau < 180°$). For measuring relaxation times shorter than 160×10^{-3} s, minimum delay time τ was approximately 100×10^{-3} s; τ was sometimes reduced to 60×10^{-3} s.

To measure T_2 under a slowly changing magnetic field, the ^{1}H-NMR spectra were recorded at different times τ of the delay between 90-degree and 180-degree pulses. The dependence of the NMR line amplitudes on the delay time τ is described by the following exponential formula

$$A = A_0 \exp\left(-\frac{2\tau}{T_2}\right). \tag{9}$$

Using this formula, T_2 can be calculated.

In Ref. [70], a model for the calculation of the thickness (h) of a monomolecular layer of adsorbed water was proposed. The model implies that the water adsorbed by a piece of coal can be divided into surface layer (so-called monolayer) that directly interacts with the surface of a solid, and the bulk water [72 – 76]. Based on this model it is assumed that a short-range interaction takes place between the pores' surfaces and water molecules in the monolayer, as well as between the monolayer and the remaining (bulk) water. Therefore, the equation for the spin – spin relaxation rate can be written as follows:

$$\frac{1}{T_2} = \frac{v}{v_{\text{s}}}\,\frac{1}{T_{\text{s}}} + \frac{v - v_{\text{s}}}{v}\,\frac{1}{T_{\text{b}}}\,, \tag{10}$$

where T_{s} and T_{b} stand for the transverse relaxation times for surface and bulk water, respectively (the subscript '2' is omitted for convenience), v is the volume of fluid in the pore, and v_{s} is the volume of fluid in the surface layer around the pore. It is suggested here that $T_{\text{s}} \ll T_{\text{b}}$, and the thickness of the layer h is close to the intermolecular distance by an order of magnitude, due to the fact that interaction between water molecules and the walls of the pore is of the nuclear dipole – dipole type with the strength being proportional to r^{-3}.

As a result of simple rearrangements, the following dependence can be obtained:

$$T_2 = \frac{v}{v_{\text{s}}}\,T_{\text{s}}\left[1 + \frac{v - v_{\text{s}}}{v}\,\frac{T_{\text{s}}}{T_{\text{b}}}\right]^{-1}. \tag{11}$$

Taking into account that $T_{\text{s}} \ll T_{\text{b}}$, one finds

$$T_2 = \frac{v}{v_{\text{s}}}\,T_{\text{s}}\,. \tag{12}$$

If a sample possesses only the same-sized pores and they are homogeneously filled with fluid, then the induced nuclear magnetization will exponentially decay in time, with the transverse relaxation time being equal to

$$T_2 = \frac{V}{V_s} T_s , \tag{13}$$

where V is the volume of fluid in the sample, and V_s is the volume of fluid in the surface layers of all pores. Equation (13) is valid only for $V \geqslant V_s$. If local ratios T_s/T_b considerably vary due to the heterogeneous distribution of fluid, or due to the different sizes of pores, or if the condition of fast intermolecular exchange is not being met, then the resulting T_2 values will be distinct in different parts of the sample. In this case, the nuclear magnetization will not decay exponentially, being in reality a sum of exponential dependences with different T_2 values. In this case, formula (13) would give the average value of T_2.

Supposing the liquid volume in a sample is gradually reduced to $V = V_S$ (V_S is the volume of the first monolayer) and taking into account that $V_S = hS$ (S being the total surface area of pores in the sample), equation (13) can be rewritten as

$$T_2 = \frac{V}{S} \frac{T_S}{h} . \tag{14}$$

It is implied that the surface area of the mono-molecular layer is identical in value to the total surface area of pores — that is, no dry pores appear as the sample dries up.

According to equations (13) and (14), the relaxation time is proportional to the volume of water contained in the sample. To verify the above dependences obtained theoretically, following experimental data were analyzed. The dependence of the relaxation time T_2 on the relative moisture content of the sample, i.e., on the V/V_0 ratio, was plotted, where V is the current volume of water in the sample, and V_0 is the maximum water volume (when all the pores are filled to the top), obviously equal to the total volume of pores.

Figure 7 shows the experimentally obtained dependence of T_2 on the relative water content of silica gels with pores 0.9 nm in radius [69]. Experimental data were approximated by two straight lines. The line for higher volumes follows the theoretical dependence (13) and passes through the origin of the coordinates. At low water content in the sample, T_2 changes due to the reduction in the number of water molecules in the first monomolecular layer, with water molecules interactions and correlation times being changed [65].

The experimental data at low moisture content in the sample were arbitrarily approximated with a straight line. The intersection point of the two straight lines should be considered as the boundary of the virtual monolayer. All approximations described above were made by means of minimization of the root-mean-square error. As can be seen from the graph (Fig. 7), there is a quite good correlation between experimental data and theoretical dependence (13).

Using equation (13), the transverse (spin–spin) relaxation time for a fully filled monolayer was calculated from the graph to be equal to $T_2 = 200 \times 10^{-6}$ s, and the amount of water that fully fills up the monomolecular layer was determined to be $V_S = 0.31\, V_0$, or $V_S = 6.6 \times 10^{-5}$ m^3 kg^{-1}, giving the thickness of the layer $h = 0.103$ nm.

The dependence of the spin–spin relaxation time T_2 on the relative water content for silica gel with pores 1.4 nm in radius is depicted in Fig. 8. This dependence is similar to the previous one, and everything said above about the behavior of T_2 for the 0.9-nm silica gel applies to it as well (apart from the numerical values). An even better correlation between the experimental data and theoretical dependence (13) can be noticed; however, at the water content on the boundary between the first and the second monomolecular layers, most experimental data appear under the theoretical line. Using the experimental data and formula (13), the following values have been obtained: $V_S = 0.11\, V_0$, i.e., $V_S = 4.2 \times 10^{-5}$ m^3 kg^{-1}, and $h = 0.084$ nm. The spin–spin relaxation time for a fully occupied monomolecular layer was also calculated to be $T_2 = 170 \times 10^{-6}$ s.

The calculated thicknesses of the first water monomolecular layer are approximately one third of the water molecule size. This fact cannot be simply explained by neglecting the curvature of pore surfaces when determining h. To prove this, an additional nuclear magnetic relaxation test was made for water adsorbed in a porous glass (with pores 1.75 nm in radius). The value of $h = 0.3$ nm was obtained while the spin–spin relaxation time for the first monomolecular layer was $T_2 = 1.1 \times 10^{-3}$ s [65]. The lower-than-expected h values obtained may be explained by the fact that water molecules in the surface layer are not evenly distributed over the whole geometrical surface, but tend to congregate around OH groups [77, 78]. This assumption goes well together with the low measured values for T_S, caused by the stronger binding of

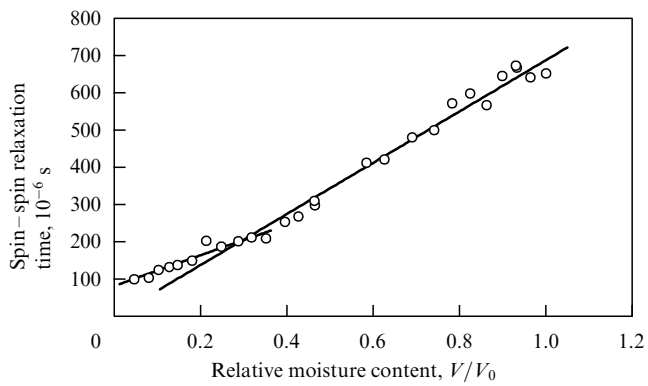

Figure 7. Dependence of the spin–spin relaxation time on the relative moisture content for silica gel with the pores 0.9 nm in radius [69].

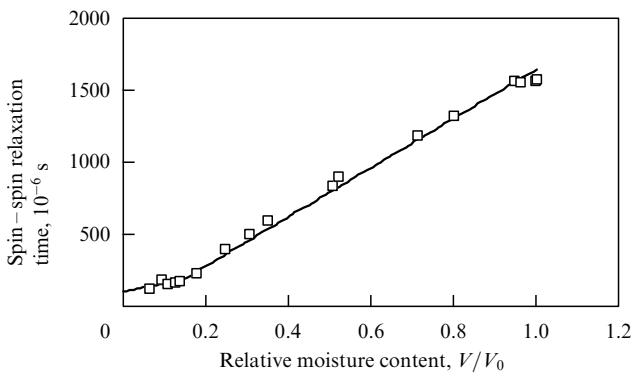

Figure 8. Dependence of the spin–spin relaxation time on the relative moisture content for silica gel with the pores 1.4 nm in radius [69].

water molecules to surface OH groups in silica gel [73]. Assuming that one molecule of water is bound to one OH group [77] and recalculating the relative volume of the monolayer (i.e., per unit of surface area) it was found that 3.5 and 2.8 hydroxyl groups, on the average, are figured to occupy each 1 nm^2 of silica gel surface with pores 0.9 and 1.4 nm in radius, respectively.

The above-described technique was employed to study the properties of moistened coals of different grades: long-flame ($V^g = 39.0\%$), blind ($V^g = 9.0\%$), and anthracite ($V^g = 5.0\%$). The highest adsorption capacity is found among long-flame coals, their water content being sometimes as high as 13%.

The relaxation time T_2 of water protons at a certain moisture content was determined from the decay of nuclear magnetization at the same moisture content using a fitting curve which is a sum of two exponents:

$$A = a \exp\left(-\frac{2\tau}{T_{2y}}\right) + b \exp\left(-\frac{2\tau}{T_2}\right), \qquad (15)$$

where T_{2y} stands for the relaxation time of coal protons, a is a constant, b and T_2 are variables, and τ is the delay time between 90-degree and 180-degree pulses. The b value is linearly dependent on the moisture content. Fitting was done until the minimum root-mean-square error was achieved.

The dependence of the relaxation time T_2 on the water content for long-flame coals with a naturally present moisture content of 13.6% (see Fig. 9) is not linear, too and can be approximated by two straight lines. As water content passes over $W = 7.5\%$, the slope of the approximation line changes, which means that water present in coal in smaller amounts is likely to form a monolayer. The spin – spin relaxation time for a fully filled monomolecular of water was calculated to be $T_2 = 120 \times 10^{-6}$ s, and the adsorption capacity of the monolayer was $\lambda = 2.31$ mol kg^{-1}. This correlates the existing data obtained earlier for long-flame coals using the adsorption isotherm technique [79].

For anthracites with $V^g = 9.0\%$, the spin – spin relaxation time T_2 for coals with the different moisture content was also determined using a fitting curve; however, instead of a constant value of T_{2y}, which was 25×10^{-6} s for the given sample, a varying constant T^*_{2y} was utilized because otherwise the experimental curve of nuclear magnetization decay could not be approximated by a sum of two exponential curves with the sufficient accuracy throughout the whole range of moisture content. The values of T^*_{2y} and T_2 obtained for different moisture contents of the A grade coal are given in Table 4 [70].

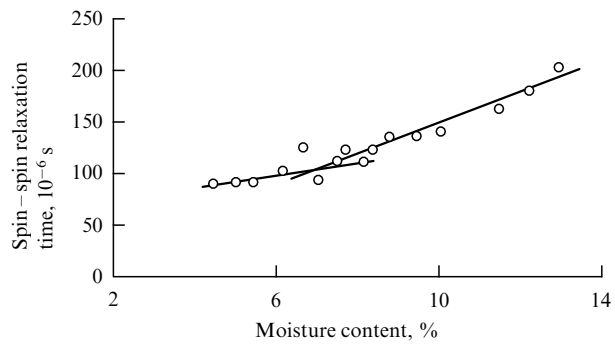

Figure 9. Dependence of the spin – spin relaxation time on the percentage of moisture content in grade L coal [70].

Table 4. The calculated spin – spin relaxation times for water and coal protons [70].

W, %	5.80	5.74	4.60	4.35	4.07	2.94	2.65	2.05
T_2, 10^{-6} s	482	447	384	360	325	203	233	190
T^*_{2y}, 10^{-6} s	36.0	35.5	34.0	31.5	30.0	28.5	27.5	27.5

The effect of varying constant T_{2y} in the first exponent of equation (15), characterizing the decay of nuclear magnetization of coal protons, could be explained as follows. In addition to open pores, closed ones are also present in coals, their total volume (for example, in anthracites) being comparable to that of open pores and sometimes exceeding it [79 – 81]. Open pores are those connected to the outer surface of a coal sample and they allow different fluids and gases to rather quickly penetrate and exit the coal mass. Closed pores of fossil coals are not connected by transport channels with the outer surface of the coal sample, and water molecules can only escape from such pores by means of solid diffusion, which is normally a very slow process.

Supposing that some water adsorbed by coal is confined in closed pores and no rapid molecular exchange between it and the water in open pores is taking place, the former should contribute to the total NMR signal of the sample. Closed pores can be very different in size — from rather small ones containing very few molecules of water, to rather large ones with significant amount of bulk water with a few molecular layers covering the pore surfaces. Thus, the relaxation time for water protons in different pores will vary from values close to T_{2y} to those close to T_2 which is the relaxation time for water protons in open pores. Closed pores that are initially filled completely would also lose water in the course of the drying process, but with some delay in time relative to open pores. Amplitudes of signals coming from water in closed pores would gradually go down, and so would the relaxation times of those signals. Time T^*_{2y} in the first exponent of equation (15), which approximates a sum of two exponents (of which one is for coal protons, and the other is for water protons in closed pores), would slowly reduce approaching to T_{2y}.

In the case of blind coal (with $V^g = 9.0\%$), the fully filled monomolecular layer corresponds to its moisture content of 2.2%, and at the higher moisture contents T_2 shows linear dependence on it. The adsorption capacity of the monomolecular layer equals $\lambda = 0.55$ mol kg^{-1}. The relaxation time for a fully filled monolayer is $T_2 = 180 \times 10^{-6}$ s. The dependence of the spin – spin relaxation time T_2 on the coal moisture content is illustrated in Fig. 10 [70].

For anthracite with $V^g = 5.0\%$, the data were obtained using the continuous method. Measured line widths were utilized for calculating the time T_2, assuming the Lorentzian shape of the NMR line. The dependence of spin – spin relaxation time plotted against coal moisture content (see Fig. 11 [71]) proved to be typically linear at high moisture values with a deviation from the straight line when the moisture content was equal to $W = 0.9$ %, corresponding to the fully filled monolayer. Time T_2 for a fully filled monolayer was 80×10^{-6} s, and the monolayer capacity $\lambda = 0.28$ mol kg^{-1}.

The results obtained from the study of silica gels as a model make possible the determination of the adsorption capacity of the virtual monolayer in fossil coals [69].

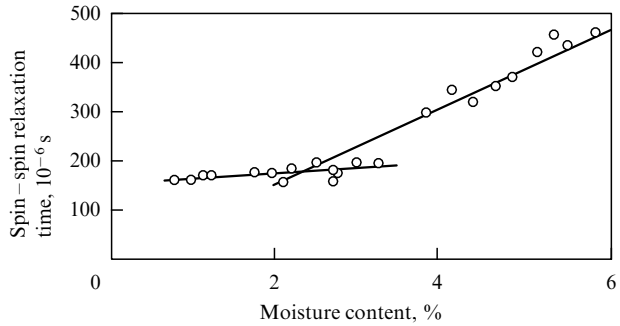

Figure 10. Spin – spin relaxation time versus moisture content in B grade coal [70].

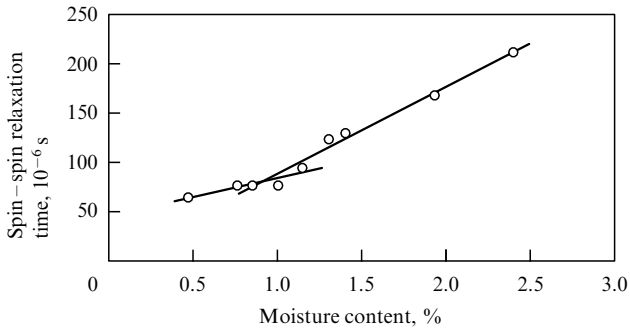

Figure 11. Spin – spin relaxation time versus moisture content for anthracite [71].

6. Application of NMR to analyzing coal – methane systems

Coal field methane is often used as a nontraditional energy source for practical purposes. In the full course of metamorphization, as coal gradually transforms from low-quality lignite to anthracite, up to 200 m^3 of methane is produced per ton of coal mass. While most of the methane diffuses into surrounding minerals and eventually passes through the ground into the outer air, a considerable part of it remains in the coal beds, the exact quantity varying from 10 to 45 $m^3\,t^{-1}$. The industrial extraction of methane incidentally with mining the major mineral (coal) therefore proves to be quite profitable [82].

The technique for the methane extraction from coal beds essentially differs from conventional technologies for extraction of gas from natural receptacles such as porous sandstones, aleurolites, and sands, because their adsorption properties are very different from those of coal. Sandstones, siltstones, and sands contain gas in the porous system comprising micropores, mesopores, and macropores [83].

The coal – methane system is out of the ordinary. The problem is that sorption by coal cannot be simply regarded as methane condensation from the gaseous phase on the pore surface. First, methane tends to fill all the volume in pores available in the coal throughout its thickness, and thus methane adsorption in coal is proportional to the volume of pores rather than to their surface. Second, as a result of metamorphization due to combined action of gas pressure and mechanical loads during the coal formation, methane deeply penetrated into the coal bed without forming chemical bonds [84]. Adsorbed methane molecules perfectly fit into empty spaces in the coal mass. Strictly speaking, in the case of the coal – methane system there is no such thing as a clear boundary between solid and gas phases and thus the concept of a sorption layer does not work. Such methane was called 'the methane in a solid solution' [85] and it takes about 80% of all sorbed methane in coal.

The application of classic sorption theories for assessing the amount of methane in coal and its behavior has been a mistake made by many researchers. For example, the authors of Refs [86 – 88] tried to describe the behavior of methane in coal assuming it was sorbed on the pore surfaces. However, due to the reasons mentioned above, the traditional determination of the amount of methane and its state based on the sorption isotherm approach introduces large errors into the results obtained. Models suggested in Refs [88 – 89] did not explain why naturally found coking and fat coals (with a relatively small porosity compared to that of other coal grades) could contain as much as 35 $m^3\ t^{-1}$ of methane.

6.1 Methane phase state in fossil coals

The use of wide-line NMR technique has made it possible to collect a wealth of information on methane behavior in coal [90 – 95]. NMR spectra of coal – methane samples [90] look very similar to those of water-saturated coals (see Fig. 3) [47]. However, the comparison of narrow-line intensities in NMR spectra of coal – methane and coal – water systems showed that the intensities of sorbed methane (I_{1m}) far exceed those of adsorbed water (I_{1w}), with the percentages of sorbed substances being the same, because the mobility of sorbed methane is much higher than that of sorbed water (see Fig. 12) [93].

For better results and the correct interpretation of measurements, it is not the values of I_{1m} and I_{1w} that should be looked at, but rather their ratios to the wide-line intensity I_2. The latter is used as a benchmark, because it remains invariable for samples of coal of the same grade [90, 93]. The standard NMR characteristics of water and methane sorbed by coal allow us to determine just what sorbate is present in a given sample of coal.

The wide-line NMR technique allows us to distinguish between methane sorbed in pores from that dissolved in a solid mass of coal, because molecules of the solid-state methane are characterized by much lower mobility. Thus, the migration of methane molecules throughout open pores (throughout narrowest filtration channels) is characterized by the diffusion coefficient $D = 10^{-8}\,m^2\,s^{-1}$, while for solid

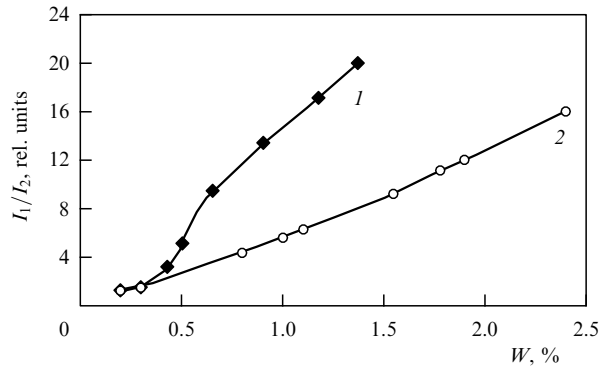

Figure 12. The NMR spectral line intensity ratio I_1/I_2 versus percentage of methane and water in anthracite: *1* — methane, *2* — water [93].

diffusion the coefficient D_m was measured to be in the interval of 10^{-12} to 10^{-16} $m^2 s^{-1}$, depending on the grade of coal.

In Refs [91, 92, 95], the research on methane desorption processes identified two phases of methane that could be characterized by different mobilities. The objects in the research were dried and de-gazed coal samples cut in the form of cylinders 20 mm long and 8 mm in diameter. This shape was chosen for better coverage of a radio-frequency loop of an NMR spectrometer (the loop was confined in a beryllium – bronze container located in the gap between magnetic poles of the NMR spectrometer). The container was filled with methane under a pressure of 10.0 MPa. The sample had been exposed to a methane environment for 10 days, until it was completely saturated with gas. As soon as the gas pressure was released, the methane desorption process started. It was noticed that during the first minutes of desorption, only the macropore and crack fractions of methane escaped from the sample. Gas sorbed by small-sized and medium-sized pores tended to disappear within a first few hours, while the rest of the methane, dissolved in the coal mass, took dozens of hours to exit the sample.

The changes in NMR spectra of methane-saturated coals illustrate the process of methane desorption from the solid coal – methane solution. An example of such a spectrum taken in conditions most favorable for tracing both the wide and narrow components is shown in Fig. 13a [90]. As mentioned above, the structure of coal – methane NMR spectra are similar to those of coal – water systems. Detailed analysis based on a specially developed computation model [96] suggests that the narrow NMR line also has a complex structure (see Fig. 13b) [90, 95]. It can be broken up into two components having different widths $\Delta H_3 = 47.7 - 79.6$ A m^{-1} and $\Delta H_4 = 7.9 - 15.9$ A m^{-1}, corresponding to two methane fractions differed in mobilities.

The spectral line with a ΔH_3 width originates from methane dissolved in a solid mass of coal, while the ΔH_4-wide line comes from methane sorbed in pores. The desorption of methane from coal starts immediately after the external gas pressure is released: gas molecules sorbed by the pores and cracks go first and are replaced by molecules of gas coming out of solid solution. The volume of pores and cracks (with localized free and sorbed methane) in the studied piece of coal remains constant, so it was suggested considering the amount of methane contained in them to be constant at

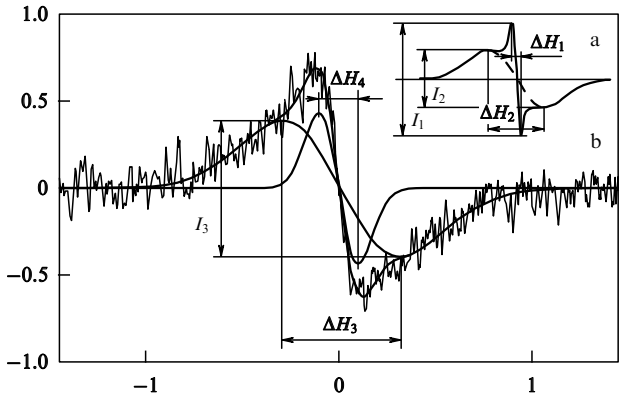

Figure 13. (a) A coal – methane NMR spectrum; (b) breakdown into components of the narrow line assigned to the overall NMR spectrum of a coal – methane system [90].

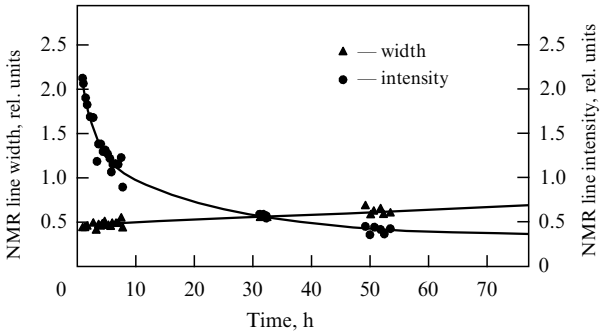

Figure 14. Width and amplitude of the coal – methane solution spectral line vs. time [95].

each instant of time as well. This means, in turn, that the number of hydrogen atoms involved in the formation of the $\Delta H_4 = 7.9 - 15.9$ A m^{-1} component of the narrow NMR line (which mathematically means the area underneath the corresponding portion of the curve) can be regarded as constant. Subtraction of the ΔH_4-component area from the total area under the narrow line curve (see Fig. 13b) gives the area under the line formed by protons in the solid coal – methane solution (ΔH_3). Using this subtraction method, the amplitude I_3 and the line width ΔH_3 for solid-state methane were calculated. Their time dependences plotted for the grade C coal ($V^g = 31.0\%$) are shown in Fig. 14 [95].

With time, the overall intensity I_3 of the corresponding line drops, its width ΔH_3 remaining largely the same. This means that even after dozens of hours from the start of degassing some methane is still dissolved in the coal. The way the intensity I_3 of the NMR signal decays with time is well suited to the commonly accepted views on the process of methane desorption out of coal.

The X-ray structural analysis done in combination with NMR spectroscopy of the same coal samples revealed changes occurring in the structure of methane-saturated coal, as opposed to dried coal [95]: the degree φ of coal structure ordering increases, other X-ray structural parameters being affected as well. In the course of desorption these parameters slowly return to their original values. This confirms the suggestion that methane tends to incorporate itself into the coal's structure, causing structural changes, and that these changes are reversible.

6.2 Methane sorption by outburst-hazardous coals

The width ΔH_1 of the narrow NMR line of methane sorbed by coal (the quantity of methane being the same) depends on the coal grade. The reason is that sorption properties of coals of different grades are distinct from each other. As coal matures, the ΔH_1 value diminishes. ΔH_1 values of NMR spectra relevant to the same grade of coal with the identical methane content are the same. This is true for samples taken from stable and outburst-safe coal beds (pillars). The analyses of samples of the same grade but taken from outburst-hazardous and outburst-safe beds have shown that the ΔH_1 value is higher for the former [17]. Thus, the narrow line width of the NMR spectrum increases by $\sim 13\%$ for grade B outburst-hazardous methane-saturated coals, and by $\sim 16\%$ for the grade C coals. This could well be explained by the results obtained with the NQR spectrometer [97], which show that in outburst-hazardous coal beds the percentage of monomer structures increases. Hence, new adsorption cen-

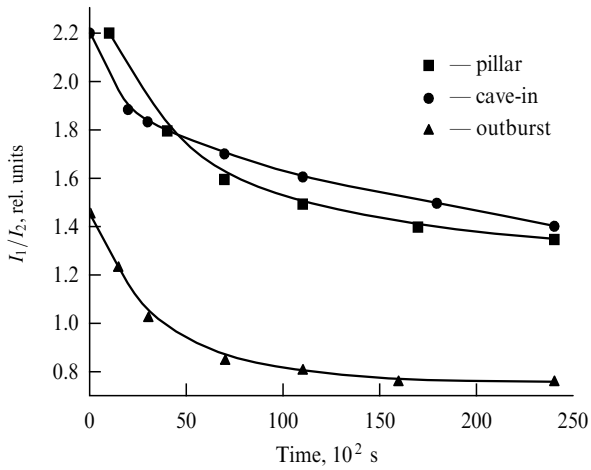

Figure 15. Changes in the intensity ratio of NMR lines for different samples of methane-saturated coals vs. desorption time [98].

ters appear that give rise to an increase in the energy of sorption interactions.

In outbursted coals, the number of sorption centers is smaller, due to the partial destruction of aliphatic structures and pores in the coal (see Section 2.3). The research work described in Refs [97, 98] has shown that if similar pieces of coal, i.e., those taken from the same bed and of the same grade, but one taken from a stable zone, and the other from an outburst zone, are saturated with methane under 10 MPA pressure, the desorption process after pressure relief would not go at the same rate. This can be clearly seen by comparison of the I_1/I_2 ratio for different samples (see Fig. 15) [98]. The graph shows that, first, outbursted coal sorbs less methane than pillar coal, and, second, desorption of methane out of it is much faster. Within 4 to 5 hours there is almost no methane left in such samples, while complete desorption from pillar coal takes several days.

The noticed differences in methane desorption rates for pillar and outbursted coal samples inspired the authors to develop a system for classification of gas- and geodynamic phenomena which is now patented [99]. It is often necessary to define the nature of the phenomenon that has taken place: whether it was a coal or gas outburst or a sudden cave-in of a steep bed of coal. As can be seen from Fig. 15, the sorption properties of coals after cave-in are not very different from those of the pillar part of the same bed, and, thus, desorption characteristics should be similar as well. This could be used as a criterion for distinguishing between caved-in and outbursted coals. In the past, physically justified criterion did not exist, and the final decision on the nature of the geodynamic phenomenon that had already taken place was made by an expert commission on site.

However, it is quite important to distinguish between different types of gas- and geodynamic phenomena to correctly plan the preventive measures to be undertaken. As a rule, to prevent sudden coal outbursts, measures should be targeted to the reduction of coal elasticity, while coal beds that tend to instant cave in already have elasticity factors quite low even before the start of coal excavation. Wrongly chosen measures can sometimes provoke or speed up unwanted gas- and geodynamic phenomena.

To test and quantify this criterion, instrumental monitoring of different gas- and geodynamic phenomena has been undertaken in coal mines of the Artemugol' and Donetskugol' coal production companies. On the basis of data collected, the following criteria was formulated:

$$B = \left(\frac{I_{1H}}{I_{2H}} - \frac{I_{1g}}{I_{2g}}\right)\left(\frac{I_{1g}}{I_{2g}}\right)^{-1},$$

where I_{1H} and I_{2H} are the intensities of the narrow and wide lines of the NMR spectrum of pillar coal, respectively, and I_{1g} and I_{2g} are the same intensities for coal after gas- and geodynamic phenomena. If the resulting value $B > 0.6$, the geodynamic phenomenon that has taken place is believed to be a sudden gas and coal outburst, while $B < 0.3$ indicates a cave-in. On the basis of these criteria, the normative document called "Means of distinction between sudden coal caving-in and outbursts for the expert's assessment of gas- and geodynamic phenomena" was developed and approved by the Ministry of Coal Industry and now is used by mining engineers.

7. Conclusion

In the past, practising mining engineers used empirical methods for the classification of the coal beds by GP types (outburst-hazardous, or dangerous to caving-in), prediction, and prevention of dangerous situations in coal mines.

Due to the successful application of NMR techniques for the analysis of coal substances and structure, a number of unknown processes taking place in coals have been discovered. Understanding these processes has helped to improve the accuracy and reliability of forecasting a methane hazard in coal mines due to coal outbursts, and has allowed the planning and undertaking of preventive measures [25, 26, 99–101].

This review was done to attract the attention of scientific circles to somewhat unusual problems caused by physical processes that proceed in fossil coals.

References

1. Waugh J S *New NMR Methods in Solid State Physics* (Cambridge: Cambridge Univ. Press, 1976) [Translated into Russian (Moscow: Mir, 1978) p. 180]
2. Malyshev Yu N, Airuni A T *Kompleksnaya Degazatsiya Ugol'nykh Shakht* (Comprehensive Degassing of Coal Mines) (Moscow: Izd. Akad. Gornykh Nauk, 1999)
3. Malyshev Yu N et al. *Metody Prognoza i Sposoby Predotvrashcheniya Vybrosov Gaza, Uglya i Porod* (Techniques of Forecast and Means of Prevention of Gas, Coal and Rock Outbursts) (Moscow: Nedra, 1995)
4. Van Krevelen D W *Coal: Typology, Chemistry, Physics, Constitution* (Amsterdam: Elsevier Publ. Co., 1961)
5. Skripchenko G B *Khim. Tverd. Topliva* (6) 18 (1984)
6. Grosberg A Yu, Khokhlov A R *Statisticheskaya Fizika Makromolekul* (Statistical Physics of Macromolecules) (Moscow: Nauka, 1989) [Translated into English (New York: AIP Press, 1994)]
7. Rus'yanova N D et al. *Khim. Tverd. Topliva* (3) 3 (1984)
8. Richards R E, Yorke R W *J. Chem. Soc.* **6** 2489 (1960)
9. Van Vleck J H *Phys. Rev.* **74** 1168 (1948)
10. Pestryakov B V *Khim. Tverd. Topliva* (4) 8 (1982)
11. Pestryakov B V, Author's synopsis of candidate thesis (Krasnoyarsk: Siberian Technological Institute, 1986)
12. Vander D L, Retcofsky H L *Fuel* **55** 202 (1976)
13. Deno N C et al. *Fuel* **60** 210 (1981)
14. Ohtsuka Y et al. *Fuel* **63** 1363 (1984)
15. Neviran R N, Davenport S J, Meinhold R H *Chem. Div. Dep. Sci. Res. Rep.* **1** 20 (1984)
16. Alexeev A D et al. *Dokl. Akad. Nauk Ukr. SSR* (3) 3 (1987)

17. Alexeev A D, Serebrova N N, Ulyanova E V *Dokl. Akad. Nauk Ukr. SSR* (9) 25 (1989)
18. Alexeev A D et al. *Radiofizika v Ugol'noi Promyshlennosti* (Radiophysics in Coal Mining) (Moscow: Nedra, 1992)
19. Tager A A *Khimiya* (1) 191 (1978)
20. Frolkov G D et al. *Khim. Tverd. Topliva* (1) 9 (1988)
21. Gagarin S G, Eremin I V, Lisurenko A V *Khim. Tverd. Topliva* (3) 3 (1997)
22. Khristianovich S A, Salganik R L, Preprint No 152 (Moscow: IPM AN SSSR, 1980)
23. Kruglitskii N I et al., in *Fisiko-Khimicheskaya Mekhanika i Liofil'nost' Dispersnykh Sistem* (Physical-Chemical Mechanics and Lyophily of Disperse Systems) Issue 13 (Ed. F D Ovcharenko) (Kiev: Naukova Dumka, 1981) p. 95
24. Alexeev A D et al. *Obrabotka Vybrosoopasnykh Plastov Vodnymi Rastvorami PAV* (Treatment of Outburst-Hazardous Coal Beds with Aqueous Surfactant Solutions) (Kiev: Tekhnika, 1988)
25. Alexeev A D, Osyka E I, Todoseichuk A L, USSR Invention Certificate No. 394692; Int. Cl. G01 3108 (1973)
26. Alexeev A D, Nedodaev N B, USSR Invention Certificate No. 756034; Int. Cl. E 21 F 5/00 (1980)
27. Gibbs J W *Elementary Principles in Statistical Mechanics* (New York: Dover Publ., 1960) [Translated into Russian (Moscow: Nauka, 1982)]
28. Randles J E *Phys. Chem. Liquids* **7** (1/2) 107 (1977)
29. Clifford J, in *Water: a Comprehensive Treatise* Vol. 5 (Ed. F Franks) (New York: Plenum Press, 1975)
30. Dubinin M M *Izv. Akad. Nauk SSSR. Ser. Khim.* (5) 996 (1974)
31. Croxton C A *Statistical Mechanics of the Liquid Surface* (Chichester: Wiley, 1980)
32. Henniker J C *Rev. Mod. Phys.* **21** 322 (1949)
33. Etzler F M, Drost-Hansen W, in *Colloid and Interface Science: Proc. of the Intern. Conf. on Colloids and Surfaces, 50th Colloid and Surface Science Symp., San Juan, Puerto Rico, June 21 – 25, 1976* Vol. 8 (Ed. M Kerker) (New York: Academic Press, 1976) p. 517
34. Mank V V, Lebovka N I, in *Fisiko-Khimicheskaya Mekhanika i Liofil'nost' Dispersnykh Sistem* (Physics, Chemistry and Mechanics of Lyophily of Disperse Systems) Issue 16 (Ed. F D Ovcharenko) (Kiev: Naukova Dumka, 1984) p. 38
35. Rideal E K *Concepts in Catalysis* (London: Academic Press, 1968) [Translated into Russian (Moscow: Mir, 1971)]
36. De Boer J H *The Dynamical Character of Adsorption* (Oxford: Clarendon Press, 1953) [Translated into Russian (Moscow: IL, 1962)]
37. Scholten J J F, Kruyer S "Some recent applications of the calculation of the entropy of the adsorbed phase according to de Boer", in *Physical and Chemical Aspects of Adsorbents and Catalysts* (Ed. B G Linsen) (London: Academic Press, 1970) [Translated into Russian (Moscow: Mir, 1973) p. 168]
38. Frenkel' Ya I *Kineticheskaya Teoriya Zhidkostei* (Kinetic Theory of Liquids) (Leningrad: Nauka, 1975) p. 592 [Translated into English (Oxford: The Clarendon Press, 1946)]
39. De Boer J H, in *Advances in Catalysis and Related Subjects* Vol. 8 (Eds W Frankenburg et al.) (New York: Wiley, 1956) [Translated into Russian (Moscow: IL, 1959) p. 18]
40. Everret D I *Proc. Chem. Soc.* **2** 38 (1957)
41. Tarasevich Yu I, in *Fisiko-Khimicheskaya Mekhanika i Liofil'nost' Dispersnykh Sistem* (Physical, Chemical Mechanics and Lyophily of Disperse Systems) Issue 16 (Ed. F D Ovcharenko) (Kiev: Naukova Dumka, 1984) p. 28
42. Gabuda S P, Rzhavin A F *Yadernyi Magnitnyi Rezonans v Kristallogidratakh i Gidratirovannykh Belkakh* (NMR Spectroscopy of Crystallohydrates and Hydrated Proteins) (Novosibirsk: Nauka, 1978)
43. Mank V V *Ukr. Khim. Zh.* **43** 911 (1978)
44. Gabuda S P *Dokl. Akad. Nauk SSSR* **143** 840 (1962)
45. Lundin A G, Fedin E I *YaMR-Spektroskopiya* (NMR Spectroscopy) (Moscow: Nauka, 1986) p. 172
46. Abragam A *The Principles of Nuclear Magnetism* (Oxford: Clarendon Press, 1961) [Translated into Russian (Moscow: IL, 1963)]
47. Alexeev A D, Morozenko E V, Serebrova N N *Dokl. Akad. Nauk Ukr. SSR* (8) 630 (1979)
48. Poole Ch P (Jr) *Electron Spin Resonance. A Comprehensive Treatise on Experimental Techniques* (New York: Interscience Publ., 1967) [Translated into Russian (Moscow: Mir, 1970)]
49. Alexeev A D et al. *Fiz.-Tekh. Problemy Razrabotki Poleznykh Iskopaemykh* (2) 11 (1970)
50. Neuman P S, Pratt L, Richards R E *Nature* **175** 645 (1955)
51. Sanada J, Honda H, Nishioka A *J. Appl. Polymer* **19** 94 (1962)
52. Belykh L G, Skripko A L, Kuralets A O *Zavodskaya Laboratoriya* (2) 168 (1963)
53. Artemov A V, Bineev E A *Khim. Tverd. Topliva* (2) 13 (1975)
54. Alexeev A D, Starikov G P *Dokl. Akad. Nauk SSSR* **259** 1075 (1981)
55. Alexeev A D et al., Preprint (6) 61 (Donetsk: Donetsk Institute of Physics and Technology of the UkrSSR Academy of Sciences, 1983) p. 28
56. Kruglitskii N N et al. *Fisiko-Khimicheskaya Mekhanika i Liofil'nost' Dispersnykh Sistem* (Physical-Chemical Mechanics and Lyophily of Disperse Systems) Issue 13 (Ed. F D Ovcharenko) (Kiev: Naukova Dumka, 1981) p. 95
57. Ulyanova E V, Author's synopsis of candidate thesis (Donetsk: Donetsk Institute of Physics and Technology of the UkrSSR Academy of Sciences, 1988)
58. Alexeev A D, Ulyanova E V, Shevchenko L V, in *Gornaya Geofizika: Materialy V Vsesoyuz. Seminara, 30 Oktyabrya – 2 Noyabrya 1989 g., Telavi* (Mining Geophysics. Proc. 5th All-Union Workshop held within 30 October – 2 November 1989 in Telavi) Part 1 (Ed. N R Nadirashvili) (Tbilisi: IGM AN GruzSSR, 1989) p. 75
59. Vol'kenshtein M V *Stroenie i Fizicheskie Svoistva Molekul* (Structure and Physical Properties of Molecules) (Moscow – Leningrad: Izd. AN USSR, 1955) p. 490
60. Grechishkin V S, Skripov F I, in *Paramagnitnyi Rezonans: Soveshchanie, Kazan 1959* (Paramagnetic Resonance: Kazan' 1959 Workshop) (Kazan', 1960) p. 160
61. Bloembergen N, Purcell E M, Pound R V *Phys. Rev.* **73** 679 (1948)
62. Waugh J S, Fedin E I *Fiz. Tverd. Tela* **4** 2233 (1962)
63. Alexeev A D, Krivitskaya B V, Pestryakov B V *Khim. Tverd. Topliva* (2) 94 (1977)
64. Blokh A M *Struktury Vody i Geologicheskie Protsessy* (Water Structure and Geological Processes) (Moscow: Nedra, 1969) p. 191
65. D'Orazio F, Bhattacharja S, Halperin W P *Phys. Rev. B* **42** 9810 (1990)
66. Gregg S J, Sink K *Adsorption, Surface Area and Porosity* 2nd ed. (London: Academic Press, 1982) [Translated into Russian (Moscow: Mir 1984)]
67. Banavar J R, Schwartz L M *Phys. Rev. Lett.* **58** 1411 (1987)
68. McCall K R, Guyer R A *Phys. Rev. B* **43** 808 (1991)
69. Alexeev A D et al. *Fiz. Tekhn. Vys. Davl.* **9** (4) 104 (1999)
70. Alexeev A D et al., in *Fiziko-Tekhnicheskie Problemy Gornogo Proizvodstva* (Physical and Technological Aspects of Mining) (Ed. A D Alexeev) (Donetsk: DonFTI NANU, 1999) p. 3
71. Alexeev A D, Ulyanova E V, Zavrazhin V V, in *Intern. Conf. on Physics of Liquid Matter: Modern Problems, 14 – 19 September 2001*, Abstracts (Kyiv: PLM MP, 2001) p. 106
72. Kel'tsev N V *Osnovy Adsorbtsionnoi Tekhniki* (Fundamentals of Adsorption Techniques) 2nd ed. (Moscow: Khimiya, 1984) p. 159
73. Chon S H, Seidel C *Bull. Magn. Reson.* **12** (1 – 2) 107 (1990)
74. Mank V V, Lebovka N I *Spektroskopiya Yadernogo Magnitnogo Rezonansa Vody v Geterogennykh Sistemakh* (NMR Spectroscopy of Water in Heterogeneous Systems) (Kiev: Naukova Dumka, 1988)
75. Giona M, Giustiniani M *Ind. Eng. Chem. Res.* **34** 3848 (1995)
76. McCall K R, Guyer R A, Johnson D L *Phys. Rev. B* **48** 5997 (1993)
77. Gallegos D P, Smith D M, Brinker C J *J. Colloid Interface Sci.* **124** 186 (1988)
78. Kiselev A V *Usp. Khim.* **25** 705 (1956)
79. Tarasevich Yu I, Rak V S *Kolloid. Zh.* **60** (1) 84 (1998) [*Colloid J.* **60** 79 (1998)]
80. Alexeev A D, Vasilenko T A, Ulyanova E V *Khim. Tverd. Topliva* (3) 39 (1999)
81. Alexeev A D, Vasilenko T A, Ulyanova E V *Fuel* **78** 635 (1999)
82. Airuni A T *Prognozirovanie i Predotvrashchenie Gazodinamicheskikh Yavlenii v Ugol'nykh Shakhtakh* (Forecast and Prevention of Gas-dynamic Events in Coal Mines) (Moscow: Nauka, 1987)

83. Alexeev A D, Airuni A T, Zverev I V *Fiz.-Tekh. Problemy Razrabotki Poleznykh Iskopaemykh* (3) 65 (1994)
84. Airuni A et al., in *Proc. of the 23th Intern. Conf. of Safety in Mines, Washington, DC, September 1989* (Washington, DC, 1989) p. 505
85. Alexeev A D et al., Certificate No. 9 for the Invention No. A-016 (1994)
86. Milewska-Duda J *Fuel* **66** 1570 (1987)
87. Bobin V A, Author's synopsis of doctoral thesis (Moscow: Research Institute of Comprehensive Exploitation of Mineral Resources of the Russian Academy of Sciences, 1992)
88. Harpalani S, Schraufnagel R A *Fuel* **69** 551 (1990)
89. Weishauptová Z, Medek J *Fuel* **77** 71 (1998)
90. Alexeev A D et al. *Fuel* **83** 1407 (2004)
91. Alexeev A D, Ulyanova E V, Kovriga N N, in *11th Intern. Symp. on Intercalation Compounds, May 27–31, Moscow, Russia, 2001* (Moscow, 2001) p. 200
92. Alexeev A D et al., in *Nauchnye Trudy Natsional'nogo Gornogo Universiteta* (Works of National Mining University) Vol. 15 (Ed. G G Pivnyak) (Dnepropetrovsk: NGU, 2002) p. 192
93. Alexeev A D, Ulyanova E V, Kovriga N N, in *Fiziko-Tekhnicheskie Problemy Gornogo Proizvodstva* (Physical and Technological Aspects of Mining) (Ed. A D Alexeev) (Donetsk: DonFTI NANU, 2001)
94. Alexeev A D, Vasylenko T A, Ul'yanova E V *Solid State Commun.* **130** 669 (2004)
95. Alexeev A D et al. *Fiz. Tekh. Vys. Davl.* **13** (4) 100 (2003)
96. Alexeev A D et al. *Fiz. Tekh. Vys. Davl.* **12** (1) 71 (2002)
97. Polyakov P I, Ulyanova E V, Vasilenko T A, in *Fiziko-Tekhnicheskie Problemy Gornogo Proizvodstva* (Physical and Technological Aspects of Mining) Vol. 1 (Ed. A D Alexeev) (Donetsk: DonFTI NANU, 1998) p. 16
98. Ulyanova E V, Starikov G P, Kuzyara V I *Fiz. Tekh. Vys. Davl.* (1) 67 (1995)
99. Alexeev A D, Ulyanova E V, Spozhakin A I, Ukraine Patent No. 19118, Int. Cl. E 21 F 5/00 (1993)
100. Alexeev A D et al. "Prognoz vybrosoopasnosti pri vskrytii krutykh i krutonaklonnykh plastov" ("Forecast of outburst hazards during coal bed opening"), Guidelines KD 12.10.05.01-99 (2000) p. 23
101. "Sposob otlichiya vnezapnogo obrusheniya (vysypaniya) uglya ot vybrosa dlya ekspertnoi otsenki tipa GDYa" ("Expert assessment of gas and geo-dynamic phenomena for the distinction of coal outbursts from abrupt failures (rock fragments pouring out)"), Guidelines KD 12.01.05.070-2001 (2001) p. 21